Lab on a Chip

Accepted Manuscript

ROYAL SOCIETY OF CHEMISTRY

www.rsc.org/loc

Journal Name

ARTICLE

IR-Live: Fabrication of a low-cost plastic microfluidic device for infrared spectromicroscopy of living cells

Received 00th January 20xx,
Accepted 00th January 20xx

DOI: 10.1039/x0xx00000x

www.rsc.org/

G. Birarda,[a,b] A. Ravasio,[c] M. Suryana,[c] S. Maniam,[c] H.-Y. N. Holman[a] and G. Grenci[c]

Water is a strong mid-infrared absorber, which has hindered the full exploitation of label-free and non-invasive infrared (IR) spectromicroscopy techniques for the study of living biological samples. To overcome this barrier, many researchers have built sophisticated fluidic chambers or micro-fluidic chips wherein the depth of the liquid medium in the sample compartment is limited to 10 µm or less. Here we report an innovative and simple way to fabricate plastic devices with infrared transparent view-ports enabling infrared spectromicroscopy of living biological samples; therefore the device is named "IR-Live". Advantages of this approach include lower production costs, a minimal need to access a micro-fabrication facility, and unlimited mass or waste exchange for the living samples surrounding the view-port area. We demonstrate that the low-cost IR-Live in combination with microfluidic perfusion techniques enables long term (> 60 h) cell culture, which broadens the capability of IR spectral microscopy for studying living biological samples. To illustrate this, we first applied the device to study protein and lipid polarity in migrating REF52 fibroblasts by collecting 2-dimensional spectral chemical maps at a micrometer spatial resolution. Then, we demonstrated the suitability of our approach to study dynamic cellular events by collecting a time series of spectral maps of U937 monocytes during the early stage of cell attachment to a bio-compatible surface.

Introduction

A major breakthrough in life science research during the last several decades is live cell imaging. Time-lapse microscopy[1], light microscopy[2], and in particular fluorescent microscopy have advanced to allow imaging beyond the diffraction limit thanks to the development of techniques like structured illumination microscopy (SIM), stimulated emission depletion (STED) microscopy, photo-activated localization microscopy (PALM) or stochastic optical reconstruction microscopy (STORM)[3-7]. Belonging to the family of chemical microscopy techniques, infrared spectromicroscopy (FTIR) uses visible light to identify the morphology of the cells or tissues and the infrared (IR) light illumination and interferometer to produce correlated chemical maps. Illumination with infrared light promotes energy exchanges between the inherent vibrational modes of molecular bonds and incident photons. These exchanges result in distinct, fingerprint-like spectral bands that appear in absorption measured as a function of wavelength of incident light (typically expressed in units of wavenumber, cm^{-1}), while the energy exchanges in the form of heat is negligible. The precise position, line shape, and intensity of infrared absorption bands depend on the molecular structure and conformation as well as intra- and inter- molecular interactions[8]. FTIR spectromicroscopy is therefore an imaging technique that is intrinsically label-free and requires minimal sample preparation. It also causes no detectable sample damage since the energy level of the infrared photons is not strong enough to break chemical bonds[9]. Thus, FTIR together with bright field microscopy and Raman spectroscopy is among the least invasive optical technique available.

In recent years, FTIR spectromicroscopy witnessed major important advancements[10-12], particularly the development of bright sources like Synchrotrons[13, 14] and tunable quantum cascade lasers[15, 16]. Importantly, advances in the detector technologies such as Focal Plane Arrays (FPA)[17, 18] have enhanced the spatial resolution up to and beyond the diffraction limit (≤ 1 µm in the mid-IR range, 400-4000 cm^{-1}).

The main technical constraint in using infrared techniques to measure living biological samples is the overwhelmingly strong water signal[19, 20]. For years a common approach was to only use FTIR to analyze dry or fixed biological samples, thereby completely removing the water absorption signal and its interference with the sample spectrum. However, this approach precludes the possibility to study live samples, such as cells maintained in culture media. To overcome this obstacle, several groups introduced microfluidic devices[21-27] or confined liquid compartments[28] which has enabled investigation of cellular processes such as cellular death,[29] cell

[a] Berkeley Synchrotron Infrared Structural Biology Program, Lawrence Berkeley National Laboratory, 1 Cyclotron road, 94720 Berkeley, USA.
[b] Elettra – Sincrotrone Trieste, Strada Statale 14 - km 163,5 in AREA Science Park, 34149 Basovizza, Trieste Italy.
[c] Mechanobiology Institute (MBI), National University of Singapore, 5A Engineering Drive 1, 117411 Singapore, Singapore.
† Footnotes relating to the title and/or authors should appear here.
Electronic Supplementary Information (ESI) available: [details of any supplementary information available should be included here]. See DOI: 10.1039/x0xx00000x

cycle progression,[30] stem cell differentiation[31] or protein misfolding[32] at the single cell level and even with a subcellular spatial resolution[33]. However, the strategies adopted so far are often hampered by slow and expensive fabrication processes[26, 34] leading to limited experimental flexibility[35].

Here we present a new type of IR compatible microfluidic device, the *IR-Live* chip, which aims to lower the cost and minimize the need to use an advanced microfabrication facility. With the exception of the initial standard lithographic step that is required to produce a reusable mould, the subsequent fabrication of a completely sealed closed-channel plastic microfluidic device featuring UV-VIS-IR transparent view-ports can be conducted in any laboratory equipped with an UV source. This new class of IR-compatible microfluidic device couples the benefits of using biocompatible polymers for the device's main body (e.g. easy connectivity to external systems, cheap and fast production, up-scalability) with high optical performance within the view-port. To demonstrate the capability of IR-Live, we used an established rat embryo fibroblast cell line (REF52) as a model system. We first confirmed the ability of IR-Live to maintain cells in culture over 60 hours. Then we demonstrated the potential of IR-Live to minimize water-absorption interference while recording high-quality infrared spectra of the cells. We collected high spatial resolution chemical maps of migrating REF52 fibroblasts and analyzed them at the cellular and subcellular scale. Following this, we imaged U937 monocytes (a human leukemic monocyte lymphoma cell line) at three consecutive time points during their adaptation to the IR-Live chamber.

Materials and Methods

IR-Live device fabrication

The principle and detailed method of the device fabrication are described in the "Results" section. Briefly, a silicon master mould was prepared by UV lithography and silicon dry etching in an inductively coupled plasma (ICP) etching tool (SPTS Technologies Ltd., Ringland Way, Newport, NP18 2TA, UK). Then the master mould was replicated to generate a working one made of polydimethylsiloxane (PDMS) (184 Sylgard, Dow Corning MIDLAND, MI 48686-0994, USA). For the main body of the IR-Live, we used the optically clear liquid adhesive NOA 73 (Norland Adhesives, 2540 Route 130, Suite 100 Cranbury, NJ 08512, USA) as the liquid UV-curable resin and IR-grade CaF_2 crystals were used for the view-ports (Crystran Ltd, 1 Broom Road Business Park Poole, Dorset, BH12 4PA, UK). The device was connected to the external pumps via metallic pins from New England Small tubes (Litchfield Technology Park, 480 Charles Bancroft Hwy., Litchfield, NH 03052, USA) and Eppendorf plastic tubes (Eppendorf AG, Barkhausenweg 1 22339 Hamburg, Germany). The flow in the device was provided by a NE 1000 syringe pump (New Era Pump Systems, Inc., 138 Toledo Street Farmingdale, NY 11735-6625, USA).

Cell culture and sample preparation

For the first set of experiments, adherent fibroblast REF52 cells were cultured in a 37 ^{o}C humidified incubator with 5% CO_2 on cell culture petri dishes with Dulbecco's Modified Eagle Medium (DMEM) supplemented with 10% fetal calf serum (FCS). Attached cells were passaged every 2-to-3 days by ethylenediaminetetraacetic acid (EDTA)/Trypsin method. For infrared experiments, cells were detached from the petri dish by the EDTA/Trypsin method. Cells were then pelleted by centrifugation (1000 rpm for 3 min) to remove cell debris and trypsin, and then re-suspended in 1 ml of fresh DMEM medium with FCS. 100 µL of the cell suspension (~500.000 cells/mL) was transferred to the IR-Live device's reservoir. Using a syringe, negative pressure was applied from the outlet to the device to draw cells into the chamber. For the second set of experiments, the monocyte cell line U937 (American Type Culture Collection, Rockville, Md, USA[36]) was cultured in RPMI 1640 medium supplemented with 10% Fetal Bovine Serum (FBS), 2 mM L-glutamine and penicillin–streptomycin (100 U/mL). Cells were maintained in an incubator at 37 ^{o}C with 5% CO_2 and cell passage was routinely done every three days. Before the experiment, cells were harvested, centrifuged at 500 rpm and suspended in fresh RPMI medium at a concentration of $1x10^6$ cells/mL. U937 cells were then transferred into the fluidic IR-Live device as described above.

Viability tests

Cell viability was accessed by means of a Calcein retention/ Ethidium Homodimer-1 exclusion assay (LIVE/DEAD Viability/Cytotoxicity Kit, Thermo Fisher Scientific). For comparison, REF52 cells were cultured for 24h either on a CaF_2 crystal inside a standard petri dish with 5 ml of growth medium placed inside an incubator (37 °C, 5% CO_2), or cultured inside an enclosed IR-Live device under static conditions, or cultured inside an enclosed IR-Live device connected to a perfused system using a IM-Q BioStation (Nikon Corporation, Japan). Then, cells were treated with Calcein (2 µM) and Ethidium Homodimer-1 (5 µM). After an additional 30-min incubation with Calcein and Ethidium Homodimer-1, the medium was replaced by the HEPES-buffered saline solution. Images were acquired using an Olympus IX71 microscope equipped with a 4x objective.

FTIR Spectral Imaging and Analysis

Infrared experiments were carried out at the Berkeley Synchrotron Infrared Structural Biology (BSISB) program facility at Advanced Light Source (ALS) beamline 5.4. Infrared images were acquired using a Hyperion 3000 IR VIS microscope equipped with high power mid-IR source (W546/8V glowbar) and a 128x128 photovoltaic MCT Focal Plane Array (FPA) detector, which were coupled to a Vertex70V interferometer (Bruker Optik Gmbh – Ettlingen, Germany). For the first experiment, which was designed to demonstrate the ability of the IR-Live to acquire chemical maps of REF52 cells with micrometer spatial resolution, we selected a 36x Schwarzschild objective/condenser pair (0.5 N.A.), resulting in a pixel size (and spatial resolution) of 1.1x1.1 μm^2. For the second

experiment, which was designed to demonstrate the potential application of the IR-Live to measure the dynamics of biochemical processes in U937 cells, we used a 15x 0.5 N.A objective granting a pixel size of 2.5x2.5 μm^2. Infrared spectral images were acquired by co-adding 512 scans per frame for REF52, and 256 scans per frame for U937 cells with 4 cm^{-1} spectral resolution, for a total acquisition time of 20 minutes or a temporal resolution of 10 minutes, respectively. Images of an empty chamber were acquired for background correction. IR images of cells were acquired using the same parameters. Image analysis was done using OPUS 7.2 software (Bruker Optik Gmbh – Ettlingen, Germany), which provided a standard pre-processing procedure to remove atmospheric water vapor and to make baseline correction via a rubber band algorithm with 5 iterations. Spectral contributions from aqueous culture media were removed by subtraction using a scaling factor proportional to the combination band (the bending vibration plus libration) of water (centered at 2150 cm^{-1})[19, 20]. Chemical maps were processed using R software and the hyperSpec package[37], converted to a specified output using ENVI to generate baseline corrected data. Further image processing and analysis were performed using ImageJ. Data were analyzed further using Excel (Microsoft Office) and Prism (GraphPad). Chemical images of proteins (Amide II 1480-1600 cm^{-1}), lipids (2800-3000 cm^{-1}), DNA (asymmetric stretching of phosphate band 1190-1260 cm^{-1}) and RNA (1160-1100 cm^{-1}, component of the symmetric stretching of the phosphate band) were obtained by integrating the respective peak area inside spectral regions, and shown as false color maps. Principal component analysis (PCA) was used to evaluate the chemical changes experienced within the cells after a 24h period inside the device, the analysis was carried out using R and the spectral regions of interest were the lipid region (2800-3000 cm^{-1}) and the one of proteins (1480-1700 cm^{-1}).

Results and discussion

IR-Live device - fabrication and characterization

Figure 1 depicts the fabrication procedure. The PDMS working mould (Figure 1.a) was prepared as a cast replica of a silicon primary master via a standard photolithography methodology. We used a dry-etched silicon primary master with the purpose of increasing its lifetime. Nonetheless, for ease of fabrication, a perfectly equivalent primary master can be prepared in a single step through UV lithography, as shown in the Supplementary (ESI Fig. 1).

The PDMS replica mould features the microfluidic circuit in the form of a 10 µm height protrusion; we used a very simple lay-out as a proof of principle, with a 5 mm wide circular central chamber accessed by an in-let channel (300 µm wide) and a similar out-let channel.

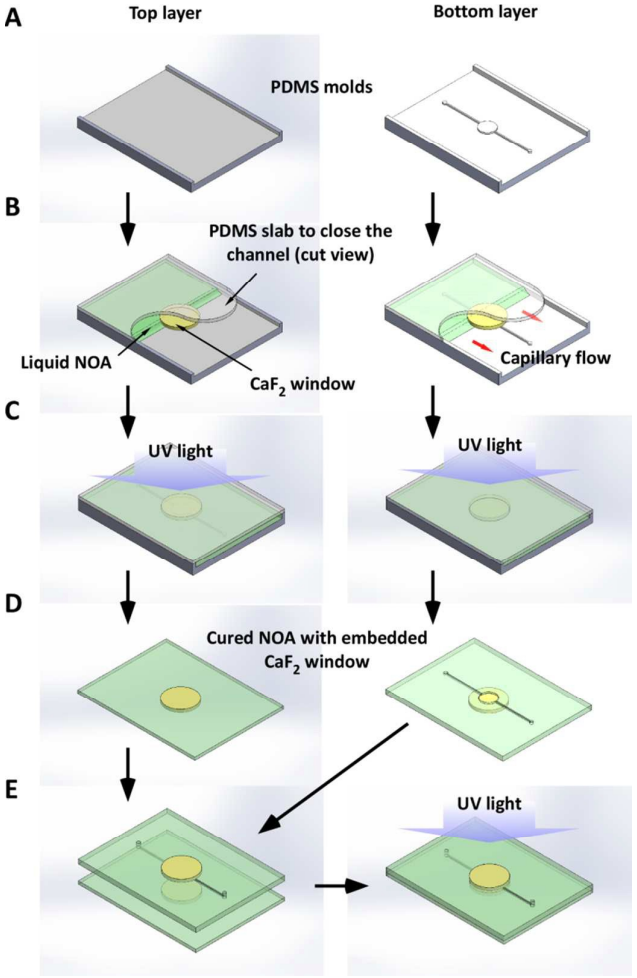

Figure 1. Schematic of the proposed fabrication procedure. A) PDMS moulds are prepared for bottom and top layers; the bottom layer (left) is a simple flat slab while the top one (right) carries the fluidic structures as protrusions 10 µm thick. Each mould features a frame 1 mm thick to define the final size and shape of the device. B) CaF_2 windows are placed in contact with the moulds and a flat PDMS cut is added to close the channel, which is filled with liquid NOA by capillarity. C) After complete filling, NOA is UV-cured. D) the solidified NOA is peeled off from its PDMS mould; on the structured half, holes are drilled corresponding to the in- and out-let of the fluidic lay-out. E) the two NOA halves are brought in contact, gently pressed and further exposed to UV light to improve adhesion.

A CaF_2 window (10 mm diameter and 1 mm thick) was sandwiched between the mould and a flat cut of PDMS (Figure 1A-B). About 0.5 ml of liquid NOA polymer was deposited on a short side of the sandwich and allowed to infiltrate by capillarity (Figure 1B). The assembly was exposed to UV light for 30s (Hg arc lamp, with an average intensity of 10 mJ/cm^2 at 365 nm) to partially cure the NOA. After peeling off from the PDMS master, holes aligned to the ends of the microfluidic channels were punched (ESI Fig. 2). The resulting slab will serve as the top part of the final device. Using the same procedure, a second CaF_2 window was embedded in a flat NOA slab to produce the unstructured bottom half (Figure 1C). Finally the two halves were pressed together and further exposed for 10 min, in order to terminate the curing of NOA and bond the device (Figure 1D). The connection to the inlet of

the pumping system was produced by inserting and gluing (with more NOA) a metallic pin into one of the openings. On the outlet, a plastic reservoir was mounted to serve as waste collector (see Figure 2A). After sealing with more glue, the device was checked for leaks with a fluorescent probe. This involved filling the IR-Live device with a dilute solution of Fluorescein (0.01 mg/mL), and imaging the device at 4x magnification with an Olympus IX71 microscope (Figure 2B). Furthermore, IR spectral imaging of the spatial distribution of water absorption intensity was used to confirm the achievement of a good seal (ESI Fig. 3). IR maps also demonstrate the absence of any interference arising from polymer.

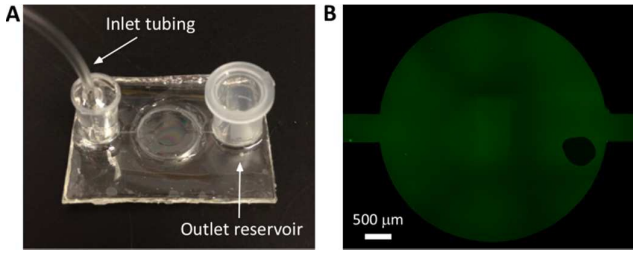

Figure 2. A) The IR-Live device with a white inlet tubing and outlet attached to the reservoir. In the centre of the device is the IR-transparent experimental chamber sandwiched between two CaF_2 crystal discs. B) A mosaic image of the central chamber of the IR-Live device, which was filled with a Fluorescein solution (0.01 mg/mL). The black spot in the chamber is a small air bubble trapped in the device for the purpose of contrasting illustration.

Cell viability within the IR-Live device

All materials used in the construction of the IR-Live chip are known to be biocompatible[38, 39]. However, a concern was whether the required 10-µm height would introduce sufficient mechanical stress to affect the cells' viability or other behavior.

To address the first concern of viability, we first cultured REF52 cells under three different conditions: On an open CaF_2 window embedded in a NOA73 slab (ESI Fig. 4); in an IR-Live device and cultured at 37 °C without medium exchange for 24 h, or in an IR-Live device with a continuous medium exchange at a flow rate of 8 µl/h for > 60 h at 37 °C, 5% CO_2. Results from the Calcein retention/ Ethidium Homodimer-1 exclusion assay showed that a large majority of cells (99.68% ± 0.44) appeared to be alive under the first culture condition (Fig. 3A).

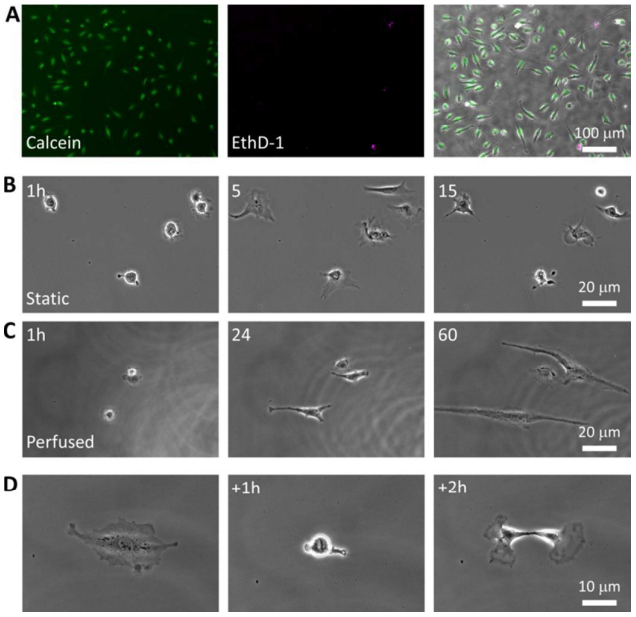

Figure 3. Results of viability tests. A) REF52 cells cultured on a CaF_2 substrate embedded in NOA73 are stained with Calcein (green) and Ethidium Homodimer-1 (red). Retention of Calcein indicates the presence of live, metabolically-active cells. Red staining of the nucleus occurs only in dead cells where the cell membrane is damaged. B) Cells grown in a closed IR-Live device is static conditions (i.e. without exchange of medium). The small, confined environment allows cells to survive only for less than 15 h. After that time, near synchronous apoptosis occurred for all cells under observation. C) Cells grown under perfused conditions (i.e. subject to continuous flow of fresh medium) survived for the entire period of observation (>60 h). D) Under perfused conditions, cells were able to perform physiological function such as mitosis and cell migration.

Next, we assessed the morphology and behavior of cells injected into the fully sealed IR-Live device by observing them in a Nikon IM-Q Biostation, a microscope equipped with an environmental chamber which maintains optimal culturing conditions (37 °C and 5% CO_2). Tests were performed under static conditions (i.e. without exchange of medium) and perfusion (flow rate = 8 µl/hr, allowing 100% medium exchange in the recording chamber every minute). For both conditions, the IR-Live device filled with medium was placed inside the environmental chamber for 2 hours to allow equilibration of temperature and CO_2 before introducing the microliter cell suspension (ESI Figure 5). Under static conditions (Fig. 3B), cells spread and attached to the CaF_2 surface within an hour. After 5 hours, cells exhibited a polarized morphology and started migrating. However, after 14 hours, cell death occurred due to a lack of nutrients and presumably an accumulation of metabolic byproducts (ESI movie 1). In perfusion conditions, a CO_2-permeable silicone tubing was used to connect an external syringe pump (New Era 1000NE) to the inlet of the IR-Live device since both NOA73 and CaF_2 are not permeable to gases. A total of 1 meter of silicone tubing was coiled inside the environmental chamber. After a 2-hours equilibration time, we drew in suspended cells from the outlet reservoir inside the environmental chamber into the central observation chamber. Under these conditions (Fig. 3C), cells proved to be viable and motile and we never

observed apoptotic events during the time of observation (>60 h – ESI movie 2). Furthermore, we witnessed a few mitosis events (Fig. 3D and ESI movie 3), implying that cells are cultured under optimal conditions.

High-resolution spatially resolved chemical maps of migrating REF52 fibroblast

We first demonstrated the potential utility of IR-Live as a high spatial resolution FTIR chemical imaging technique. 1 µl of REF52 cell suspension (approx. 500 to 1000 cells) was pipetted into the outlet chamber of the IR-Live device. Using a 1 mL syringe connected to the inlet tubing, cells were pulled-transferred inside the CaF_2 chamber. Thereafter, the IR-Live device was kept inside the cell culture incubator for 2 hours to allow the cells to adapt to the new conditions, and to adhere and spread onto the substrate surface. After two hours, the IR-Live device was flushed with the fresh medium to remove unattached cells and mounted on the temperature-controlled microscope stage at the IR beamline (Fig 4A). Several groups of cells were visually selected according to their shape and morphology for subsequent IR spectral imaging. We subsequently employed a 36x Schwarzschild objective/condenser pair (0.5 N.A.), which yields a pixel size of 1.1x1.1 μm^2. For each pixel within a field of view ~69 µm by 69 µm, a corresponding full spectrum of chemical absorption between 4,000 and 900 cm^{-1} was acquired (Fig 4C). By integrating the absorption peaks at the CH_2-CH_3 stretching (3,000 – 2,800 cm^{-1}) region, we obtained the spatial distribution of lipid molecules (Fig 4B). Likewise, integration of the signal in the amide II absorption envelope in the 1,600 – 1,480 cm^{-1} region was used to map the spatial distribution of proteins.

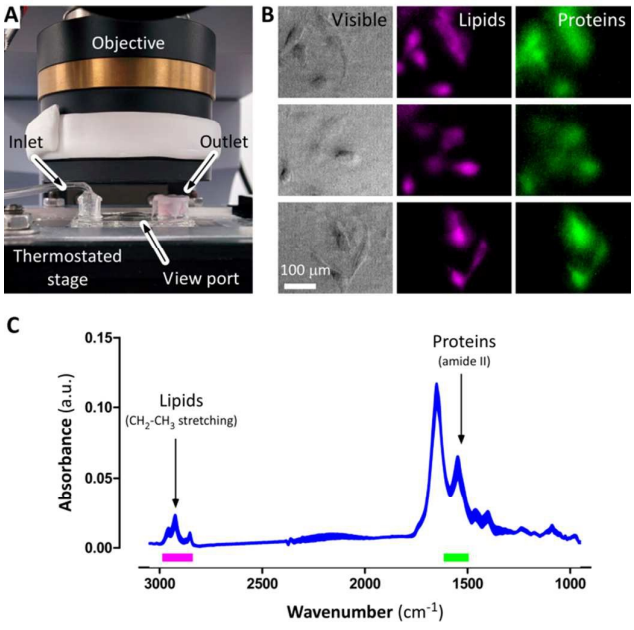

Figure 4. A) A close-up photo of the experimental setup at the BSISB infrared beamline 5.4.1 at the ALS. The IR-Live device was placed on a heating stage set at 37°C under a 36X objective lens of a Hyperion 3000 IR/VIS microscope. B) Several groups of motile REF52 cells. Visible transmitted light micrographs (bright field) and spatially resolved infrared chemical spectral heat maps of protein (magenta) and lipids (green) are shown. The Schwarzschild objectives of medium/high magnification factor do not grant a good optical contrast in the visible spectral range, therefore the quality of the bright field images generally did not contrast well and details of the migrating cell such as cellular organelles and protrusions are blurred. C) Absorption spectra of the measured cells, presented as an average spectrum ± standard deviation (n = 14 cells). Color bars represent spectral regions used to quantify lipids (magenta) and proteins (green).

Analysis of the spatially resolved distribution of proteins and lipids revealed that the REF52 cells displayed characteristic shapes of motile cells (ESI Fig 6A) with a pronounced rear-front polarity (as compared to the direction of motion). From all the spectral heat maps analyzed (Fig 4B), we identified a cell with a typical spindle shape; its morphology and rear-front polarity could be easily identified (see ESI Fig 6B). Interestingly, the chemical maps of this cell indicated a strong rear-front as well as left-right asymmetry of lipid and protein distribution (Fig 5A). In particular, the line plot starting from the rear of the cell (Fig 5B, Line 1, arrow head a) showed that both chemical species increased in abundance, an observation which is compatible with the transition between the retracting flat regions at the trailing end of the cell to the cell body. While protein absorbance increased steadily and reached a peak at x = 45 µm (Fig 5B, Line 1, arrow head c), lipids showed a transient plateau (Fig 5B, Line 1, arrow head b). This might reflect the presence at this region of the nucleus, which is mostly composed by the nucleic acids and histone protein enclosed within a single phospholipid bilayer. The spectral heat map also showed a lipid and protein rich compartment ahead of this region (Fig 5A). In most migrating cells, they translocate forward to the nucleus a large portion of the endoplasmic reticulum, the Golgi apparatus and secretory vesicles, to readily provide the migratory machinery with freshly synthesized proteins and membrane lipids. Away from this chemically rich region (Fig 5B, Line 1, arrow head d), both lipids and proteins signals sharply declined with distance until reaching a region where the protein absorbance remained dominant while the lipid absorbance nearly vanished. This would be consistent with the presence of the lamellipodium at the front of a migrating cell. This migratory structure is composed mostly of actin-binding proteins and cross-linked actin filaments that are closely associated with the cell membrane. Interestingly, this protein rich structure extended from the front to the left side of the cells (Fig 5B, Line 2, arrow head f). A finer analysis of the chemical composition of this structure revealed the following information. Point “b”, identified as belonging to the nucleus has a sharp protein signal centered at 1654 cm^{-1} which is mainly attributed to α-helix protein structure. At points “d” and “f”, located near the front of the cell, there was a 2 cm^{-1} redshift of both CH_2, respectively from 2925 cm^{-1} and 2853 cm^{-1}, to 2923 cm^{-1} and 2851 cm^{-1}. This suggests a higher lipid organization at this pole of the cell. The data suggest that there is a compartmentalization of the plasma membrane, which at the front seems to contain more ordered lipid domains relative to other regions of the cell.

To highlight the main spectral features that change after 24h inside the device, we performed a PCA analysis on data collected at t_0=0 and t_1=24h, (see ESI Fig S7). Principal component 1 mainly describes variations on the protein content, whereas principal component 2 is related more to modifications of the lipids. From this analysis we cannot observe a trend in the variation of proteins, as it was expected since the cells were not synchronized. An increase in lipids content is clear, and it can be related to the spreading of the membrane onto the surface, typical of this cell line that is known for its high motility.

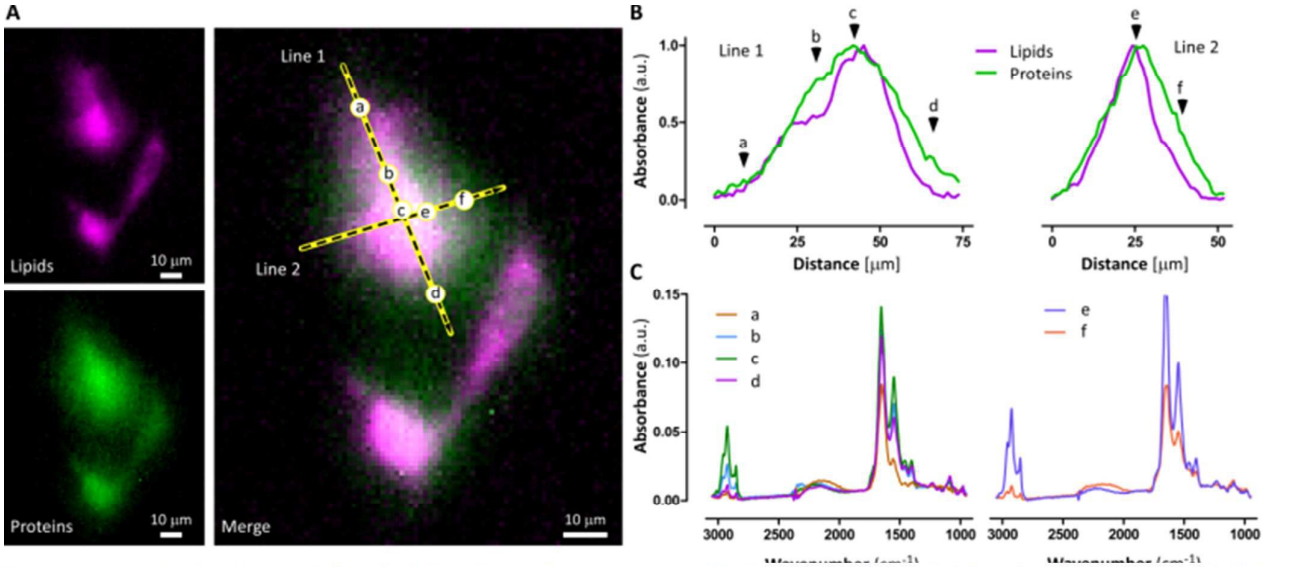

Figure 5. A) Images of high resolution spatially resolved chemical maps of protein (magenta) and lipids (green) are shown in the left panels, and merged (right panel). B) Line profiles of the integrated infrared absorbance lipids (purple) and proteins (green). The 75-µm long Line 1 starts at the trailing rear of the cell and ends at the front. Line 2 spans from the right of the cells to the left as compared to the direction of movement. To reduce random noise, the line image is an average of 4 pixels (about 4.4 µm wide). C) Adsorption spectra at different areas (4x4 pixels, about 20 µm2) within the cell.

Time-resolved chemical maps of U937 monocytes during adaptation

We also demonstrated the potential utility of the IR-Live as a real-time chemical imaging tool by performing a simple experiment imaging the transient spectral signatures of cells within the first hour of their adaptation to the IR-Live chamber after the injection. For this experiment, we used U937 monocytes. These cells are easy to inject into the device as they are quite small (~10 µm diameter). We chose a 15x objective (i.e. a pixel size of 2.62x2.62 µm^2), which was about two-fold coarser in spatial resolution than that of the experiment with REF52 cells. However, the benefits of this lower magnification are as follows: a larger field of view; higher signal-to-noise ratio; lesser number of scans required, enabling a more detailed temporal resolution. Time-course analysis of the FTIR image measurements starting with the introduction of cells into the IR-Live chamber shows a sequence of biomolecule synthesis events during the adaption of the cells to the bio-compatible surface, or the so called "settling down phase", as shown in Figures 6A-D. From comparing U937 spectra in Figure 6C with those in Figure 4C from REF52 fibroblasts, we can see some differences in the relative composition of lipids and proteins. This clearly indicates that every cell type has a slightly different IR spectrum, which is important as it demonstrates that FTIR using IR-Live provides sufficient details for cell recognition. Initially, U937 cells could have been at a resting state because of the handling process required before injection. During the first 30 minutes, we observed a ~14% increase in the intensity of the phosphodiester $\nu_{as}(PO_2^-)$ groups of phosphorylated proteins or DNA/RNA polysaccharide backbone structure (~1233 cm^{-1}) and a ~5% increase in the signal of protein amide II. An increase in the absorption intensity in the 966-930 cm^{-1} area together with an increase at ~1082 and ~1233 cm^{-1} could be attributed to protein phosphorylation[24]. In the following 30 minutes, the infrared absorption intensity of protein amide II and of lipid signals increased by ~20%. In contrast, the signals from $\nu_{as}(PO_2^-)$ groups of phosphorylated proteins reached a plateau, or even decreased slightly. This transient behavior of infrared signals of protein phosphorylation is consistent with those reported earlier[25].

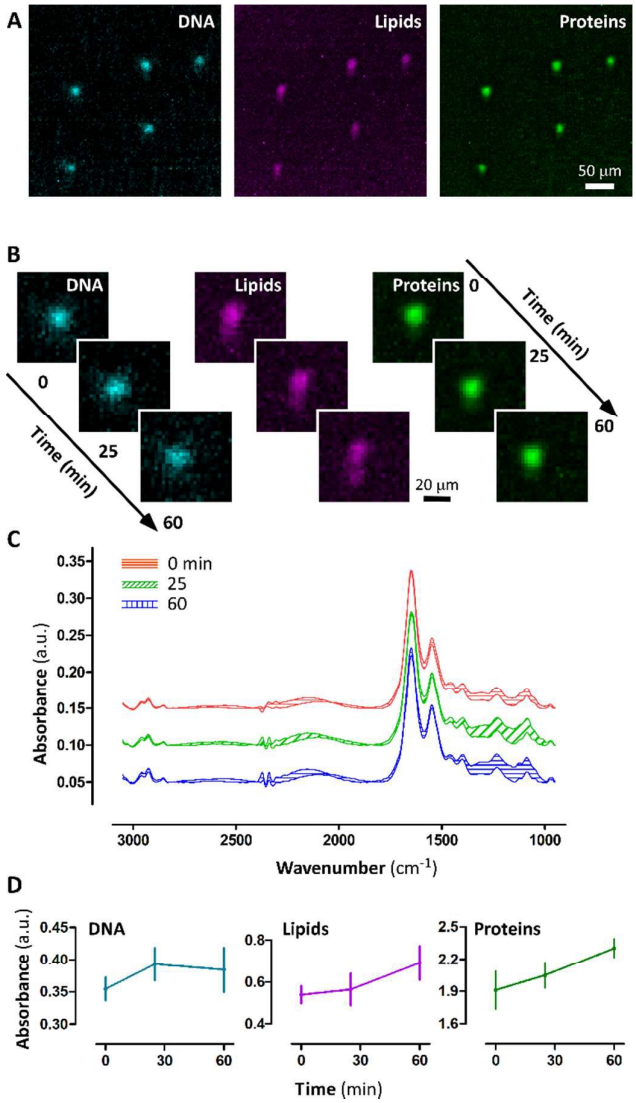

Figure 6. Spatial and temporal distributions of DNA, lipids and proteins. A) FTIR chemical maps of U937 monocytes, showing the spatial distribution of the main cellular components (DNA, lipids and proteins respectively). The acquisition time for each frame was 10 minutes. B) Time-dependent evolution of the average spectra of U937 monocytes. C) An example of time-dependent changes in cellular chemistry as expressed by the absorption spectra at different time points, each time point is expressed by an average spectrum (n=5 cells) ± a standard deviation. D) Plots of the time variation of the integrated average absorption peak intensity for protein phosphorylation, lipids, and protein contents.

Summary & Conclusions

We have demonstrated a protocol to build a low-cost IR-Live microfluidic chip for real-time 2-D infrared imaging of living cells or tissues with a spatiotemporal resolution in the range of micrometers and minutes. In previously published work[21, 40-42], FTIR compatible microfluidic chips were produced by direct photolithography of a resist layer coated onto one large IR windows (40 mm diameter). Although suitable for FTIR experiments, that approach suffered from two major drawbacks: the use of a large IR window as the whole substrate, in which holes for fluidic connections have to be directly drilled in, and the need of a photolithographic step to be performed for each single device. We argue that these limitations could reduce the general applicability of that approach to a broader community of FTIR users. Here we used a very simple microfluidic layout to demonstrate a new fabrication scheme aimed at solving these issues.

Using a plastic frame as the main body of the final IR-Live device will enable designing and building more complex microfluidic layouts for infrared imaging of living samples in real-time, since it removes the need for micromachining the IR/VIS transparent window. Most importantly, it confines the requirement of a 10-μm thick medium layer to the view-port area only. Furthermore, the fabrication approach proposed here reduces the need to access a microfabrication laboratory only for the production of a starting silicon master; all the subsequent steps also can be carried on in any lab equipped for standard soft lithography. We demonstrated that cells do not suffer in the 10-μm spatial confinement even for experiments lasting multiple days. Cells are able to attach and proliferate inside the IR-Live device if nutrients are provided and wastes are removed.

From our results of IR imaging on migrating cells with sub cellular spatial resolution, we were able to distinguish different cellular organelles and identify their peculiar chemical composition at a functional group level. We also presented results from using the IR-Live chip to unravel the behavior of cells as they were adapting to the IR-Live device. Temporal and spatial resolutions of this IR-mapping configuration can be adjusted according to a range of experimental parameters such as cell type, cell size, or signal-to-noise ratio. This novel approach will offer great, perhaps even revolutionary new capabilities for the future of infrared imaging of living biosystems in biological, microbial, or biomedical research

Acknowledgements

We acknowledge financial support from Mechanobiology Institute (MBI), National University of Singapore, through internal seed grant.

This work was performed in part under the Berkeley Synchrotron Infrared Structural Biology (BSISB) Program funded by the US Department of Energy, Office of Science, and Office of Biological and Environmental Research. The Advanced Light Source is supported by the Director, Office of Science, and Office of Basic Energy Sciences. Both were supported through Contract DE-AC02-225 05CH11231.

The authors acknowledge A. Wong and J. Shanmugarajah of the Mechanobiology Institute for help editing the manuscript.

Notes and references

1. B. Neumann, T. Walter, J. K. Heriche, J. Bulkescher, H. Erfle, C. Conrad, P. Rogers, I. Poser, M. Held, U. Liebel, C. Cetin, F. Sieckmann, G. Pau, R. Kabbe, A. Wunsche, V. Satagopam, M. H. Schmitz, C. Chapuis, D. W. Gerlich, R.

Schneider, R. Eils, W. Huber, J. M. Peters, A. A. Hyman, R. Durbin, R. Pepperkok and J. Ellenberg, *Nature*, 2010, 464, 721-727.
2. W. Choi, C. Fang-Yen, K. Badizadegan, S. Oh, N. Lue, R. R. Dasari and M. S. Feld, *Nature methods*, 2007, 4, 717-719.
3. S. W. Hell and J. Wichmann, *Optics letters*, 1994, 19, 780-782.
4. T. D. Lacoste, X. Michalet, F. Pinaud, D. S. Chemla, A. P. Alivisatos and S. Weiss, *Proceedings of the National Academy of Sciences of the United States of America*, 2000, 97, 9461-9466.
5. L. Schermelleh, P. M. Carlton, S. Haase, L. Shao, L. Winoto, P. Kner, B. Burke, M. C. Cardoso, D. A. Agard, M. G. Gustafsson, H. Leonhardt and J. W. Sedat, *Science*, 2008, 320, 1332-1336.
6. M. F. Juette, T. J. Gould, M. D. Lessard, M. J. Mlodzianoski, B. S. Nagpure, B. T. Bennett, S. T. Hess and J. Bewersdorf, *Nature methods*, 2008, 5, 527-529.
7. S. R. Pavani, M. A. Thompson, J. S. Biteen, S. J. Lord, N. Liu, R. J. Twieg, R. Piestun and W. E. Moerner, *Proceedings of the National Academy of Sciences of the United States of America*, 2009, 106, 2995-2999.
8. H. H. Mantsch and D. Chapman, *Infrared spectroscopy of biomolecules*, Wiley-Liss, New York, 1996.
9. H. Y. Holman, K. A. Bjornstad, M. P. McNamara, M. C. Martin, W. R. McKinney and E. A. Blakely, *Journal of biomedical optics*, 2002, 7, 417-424.
10. P. Dumas, G. L. Carr and G. P. Williams, *Analusis*, 2000, 28, 68-74.
11. L. M. Miller and P. Dumas, *Bba-Biomembranes*, 2006, 1758, 846-857.
12. G. L. Carr, *Rev Sci Instrum*, 2001, 72, 1613-1619.
13. M. J. Nasse, M. J. Walsh, E. C. Mattson, R. Reininger, A. Kajdacsy-Balla, V. Macias, R. Bhargava and C. J. Hirschmugl, *Nature methods*, 2011, 8, 413-U458.
14. E. Stavitski, R. J. Smith, M. W. Bourassa, A. S. Acerbo, G. L. Carr and L. M. Miller, *Anal Chem*, 2013, 85, 3599-3605.
15. K. Yeh, S. Kenkel, J. N. Liu and R. Bhargava, *Anal Chem*, 2015, 87, 485-493.
16. N. Kroger-Lui, N. Gretz, K. Haase, B. Kranzlin, S. Neudecker, A. Pucci, A. Regenscheit, A. Schonhals and W. Petrich, *The Analyst*, 2015, 140, 2086-2092.
17. E. N. Lewis, P. J. Treado, R. C. Reeder, G. M. Story, A. E. Dowrey, C. Marcott and I. W. Levin, *Anal Chem*, 1995, 67, 3377-3381.
18. R. Blanchard, S. V. Boriskina, P. Genevet, M. A. Kats, J. P. Tetienne, N. Yu, M. O. Scully, L. Dal Negro and F. Capasso, *Optics express*, 2011, 19, 22113-22124.
19. K. Rahmelow and W. Hubner, *Appl. Spectrosc.*, 1997, 51, 160-170.
20. S. Y. Venyaminov and F. G. Prendergast, *Anal Biochem*, 1997, 248, 234-245.
21. E. Mitri, G. Birarda, L. Vaccari, S. Kenig, M. Tormen and G. Grenci, *Lab Chip*, 2014, 14, 210-218.
22. L. Vaccari, G. Birarda, G. Grenci, S. Pacor and L. Businaro, *J Phys Conf Ser*, 2012, 359.
23. E. J. Marcsisin, C. M. Uttero, M. Miljkovic and M. Diem, *The Analyst*, 2010, 135, 3227-3232.
24. L. Chen, H. Y. N. Holman, Z. Hao, H. A. Bechtel, M. C. Martin, C. B. Wu and S. Chu, *Anal Chem*, 2012, 84, 4118-4125.
25. H. Y. N. Holman, H. A. Bechtel, Z. Hao and M. C. Martin, *Anal Chem*, 2010, 82, 8757-8765.
26. B. Lehmkuhl, S. D. Noblitt, A. T. Krummel and C. S. Henry, *Lab Chip*, 2015, 15, 4364-4368.
27. P. Heraud, B. R. Wood, M. J. Tobin, J. Beardall and D. McNaughton, *Fems Microbiol Lett*, 2005, 249, 219-225.
28. M. J. Nasse, S. Ratti, M. Giordano and C. J. Hirschmugl, *Appl Spectrosc*, 2009, 63, 1181-1186.
29. G. Birarda, D. E. Bedolla, E. Mitri, S. Pacor, G. Grenci and L. Vaccari, *The Analyst*, 2014, 139, 3097-3106.
30. D. E. Bedolla, S. Kenig, E. Mitri, P. Ferraris, A. Marcello, G. Grenci and L. Vaccari, *The Analyst*, 2013, 138, 4015-4021.
31. C. Sandt, J. Frederick and P. Dumas, *Journal of biophotonics*, 2013, 6, 60-72.
32. G. Hoffner, W. Andre, C. Sandt and P. Djian, *Rev Anal Chem*, 2014, 33, 231-243.
33. L. M. Miller, M. W. Bourassa and R. J. Smith, *Bba-Biomembranes*, 2013, 1828, 2339-2346.
34. G. Grenci, G. Birarda, E. Mitri, L. Businaro, S. Pacor, L. Vaccari and M. Tormen, *Microelectron Eng*, 2012, 98, 698-702.
35. M. J. Tobin, L. Puskar, R. L. Barber, E. C. Harvey, P. Heraud, B. R. Wood, K. R. Bambery, C. T. Dillon and K. L. Munro, *Vib Spectrosc*, 2010, 53, 34-38.
36. C. Sundstrom and K. Nilsson, *International journal of cancer. Journal international du cancer*, 1976, 17, 565-577.
37. C. Beleites and V. Sergo, 2011.
38. E. Sollier, C. Murray, P. Maoddi and D. Di Carlo, *Lab Chip*, 2011, 11, 3752-3765.
39. K. Wehbe, J. Filik, M. D. Frogley and G. Cinque, *Analytical and bioanalytical chemistry*, 2013, 405, 1311-1324.
40. L. Vaccari, G. Birarda, L. Businaro, S. Pacor and G. Grenci, *Anal Chem*, 2012, 84, 4768-4775.
41. G. Birarda, G. Grenci, L. Businaro, B. Marmiroli, S. Pacor and L. Vaccari, *Microelectron Eng*, 2010, 87, 806-809.
42. G. Birarda, G. Grenci, L. Businaro, B. Marmiroli, S. Pacor, F. Piccirilli and L. Vaccari, *Vib Spectrosc*, 2010, 53, 6-11.